



Residual Stress Measurements of Ni-Base Superalloys Through Neutron Diffraction

*T.M. Smith and R.W. Carter
Glenn Research Center, Cleveland, Ohio*

*K. An and Y. Chen
Oak Ridge National Laboratory, Oak Ridge, Tennessee*

*I.E. Locci
University of Toledo, Toledo, Ohio*

*R.J. Pawlik
HX5 Sierra, Fort Walton Beach, Florida*

*T.P. Gabb, J. Telesman, and L.J. Evans
Glenn Research Center, Cleveland, Ohio*

NASA STI Program . . . in Profile

Since its founding, NASA has been dedicated to the advancement of aeronautics and space science. The NASA Scientific and Technical Information (STI) Program plays a key part in helping NASA maintain this important role.

The NASA STI Program operates under the auspices of the Agency Chief Information Officer. It collects, organizes, provides for archiving, and disseminates NASA's STI. The NASA STI Program provides access to the NASA Technical Report Server—Registered (NTRS Reg) and NASA Technical Report Server—Public (NTRS) thus providing one of the largest collections of aeronautical and space science STI in the world. Results are published in both non-NASA channels and by NASA in the NASA STI Report Series, which includes the following report types:

- **TECHNICAL PUBLICATION.** Reports of completed research or a major significant phase of research that present the results of NASA programs and include extensive data or theoretical analysis. Includes compilations of significant scientific and technical data and information deemed to be of continuing reference value. NASA counter-part of peer-reviewed formal professional papers, but has less stringent limitations on manuscript length and extent of graphic presentations.
- **TECHNICAL MEMORANDUM.** Scientific and technical findings that are preliminary or of specialized interest, e.g., “quick-release” reports, working papers, and bibliographies that contain minimal annotation. Does not contain extensive analysis.
- **CONTRACTOR REPORT.** Scientific and technical findings by NASA-sponsored contractors and grantees.
- **CONFERENCE PUBLICATION.** Collected papers from scientific and technical conferences, symposia, seminars, or other meetings sponsored or co-sponsored by NASA.
- **SPECIAL PUBLICATION.** Scientific, technical, or historical information from NASA programs, projects, and missions, often concerned with subjects having substantial public interest.
- **TECHNICAL TRANSLATION.** English-language translations of foreign scientific and technical material pertinent to NASA's mission.

For more information about the NASA STI program, see the following:

- Access the NASA STI program home page at <http://www.sti.nasa.gov>
- E-mail your question to help@sti.nasa.gov
- Fax your question to the NASA STI Information Desk at 757-864-6500
- Telephone the NASA STI Information Desk at 757-864-9658
- Write to:
NASA STI Program
Mail Stop 148
NASA Langley Research Center
Hampton, VA 23681-2199



Residual Stress Measurements of Ni-Base Superalloys Through Neutron Diffraction

*T.M. Smith and R.W. Carter
Glenn Research Center, Cleveland, Ohio*

*K. An and Y. Chen
Oak Ridge National Laboratory, Oak Ridge, Tennessee*

*I.E. Locci
University of Toledo, Toledo, Ohio*

*R.J. Pawlik
HX5 Sierra, Fort Walton Beach, Florida*

*T.P. Gabb, J. Telesman, and L.J. Evans
Glenn Research Center, Cleveland, Ohio*

National Aeronautics and
Space Administration

Glenn Research Center
Cleveland, Ohio 44135

Acknowledgments

Funding for this study was provided by NASA's Aeronautics Research Mission Directorate (ARMD) Advanced Air Transport Technology (AATT) Project Office. Neutron diffraction work was carried out at the Spallation Neutron Source (SNS), which is the U.S. Department of Energy (DOE) user facility at the Oak Ridge National Laboratory, sponsored by the Scientific User Facilities Division, Office of Basic Energy Sciences.

This work was sponsored by the Advanced Air Vehicle Program
at the NASA Glenn Research Center

Trade names and trademarks are used in this report for identification
only. Their usage does not constitute an official endorsement,
either expressed or implied, by the National Aeronautics and
Space Administration.

Level of Review: This material has been technically reviewed by technical management.

Available from

NASA STI Program
Mail Stop 148
NASA Langley Research Center
Hampton, VA 23681-2199

National Technical Information Service
5285 Port Royal Road
Springfield, VA 22161
703-605-6000

This report is available in electronic form at <http://www.sti.nasa.gov/> and <http://ntrs.nasa.gov/>

Residual Stress Measurements of Ni-Base Superalloys Through Neutron Diffraction

T.M. Smith and R.W. Carter
National Aeronautics and Space Administration
Glenn Research Center
Cleveland, Ohio 44135

K. An and Y. Chen
Oak Ridge National Laboratory
Oak Ridge, Tennessee 37830

I.E. Locci
University of Toledo
Toledo, Ohio 43606

R.J. Pawlik
HX5 Sierra
Fort Walton Beach, Florida 32548

T.P. Gabb, J. Telesman, and L.J. Evans
National Aeronautics and Space Administration
Glenn Research Center
Cleveland, Ohio 44135

Abstract

Linear friction welding (LFW) is being considered for joining single crystal to polycrystalline nickel-base alloys for advanced high temperature gas turbine disks. Unfortunately, the transient thermal cycle during the welding generates undesirable residual stresses. Additionally, upon thermal treatment to relieve these residual stresses the weld joints often crack. To understand this issue, state-of-the-art neutron diffraction was performed near weld joints to quantify the residual stresses created by varying linear friction weld conditions. The residual stresses were measured along three orthogonal axes in both the polycrystalline LSHR and single crystal SC-180 alloys. Residual stress measurements using a contour method were used to compare the calculations obtained by neutron diffraction. The results suggest high residual stresses can be successfully reduced using both pre- and post-weld processing steps. Moreover, the effect of grain size and pre-heat temperatures on the LFW process were explored.

The data required to reproduce these findings is available from the corresponding author upon request.

1.0 Introduction

Reducing the CO₂ emissions in jet turbine engines has increasingly become a priority within industry and research institutions (Ref. 1). Currently Ni-base superalloys are the primary material system used in the hot section of gas turbine engines (Ref. 2). Therefore, reducing the weight of the superalloy

components or producing new optimized configurations are important objectives for future gas turbine development (Refs. 3 to 6). Presently, turbine engines are constrained to operating temperatures below 700 °C (Ref. 2). This temperature limit primarily exists in polycrystalline disk alloys due to the presence of grain boundaries which become a major source of creep and dwell fatigue damage when temperatures exceed 700 °C (Refs. 7 to 10). Conversely, these same grain boundaries provide necessary fatigue and tensile strength needed near the disk's bore where the temperatures are significantly cooler (Refs. 2 and 11). Therefore, modern turbine disks which need to operate successfully in a wide range of stresses and temperatures contain dual microstructures, where the rim of the disk have significantly larger grains compared to the bore (Refs. 12 and 13).

One solution that is currently being investigated is a hybrid disk, which consists of a single crystal rim attached to a polycrystalline turbine bore (Ref. 4). Though this configuration would further optimize the disk's overall properties, joining the single crystal and polycrystalline alloys presents significant challenges. Past studies have found Ni-base superalloys, especially single crystal versions, to be extremely difficult to weld due in part to their high volume fractions of the intermetallic γ' precipitates (Ref. 14). Linear friction welding (LFW), a novel joining technique, has recently shown promise overcoming this problem. LFW is a state-of-the-art technique which uses the heat generated by rapidly oscillating two metals together under a constant force. The resulting heat plasticizes the contacting surfaces and subsequently joins them (Ref. 15). This technique has been shown to produce reliable crack-free welds in many other difficult to weld alloys (Refs. 16 to 19). Still, a notable concern with this technique is the production of residual stress which may be prohibitive for use in jet engines (Refs. 20 and 21). In fact, safety requirements necessitate reasonable low residual stress levels for use in commercial aircraft (Ref. 22). Therefore, predicting and mitigating the residual stresses created by LFW between a polycrystalline and single crystal Ni-base superalloy is critical for incorporating hybrid disks in future turbine engine applications.

In this study, the residual stresses created along the weld joint between a polycrystalline and single crystal superalloy were measured using neutron diffraction. The effect both pre-heating and post-processing have on residual stress mitigation in LSHR and the single crystal superalloy SC-180 were investigated. Two-dimensional heat-maps of the measured residual stresses in three orthogonal directions were produced to better understand the resulting stress environment throughout the weld. The experimental stress measurements found pre-heating samples before the LFW process significantly reduced the residual stress in all three measured directions. The same result was also observed following a post-weld hot isostatic press (HIP) cycle.

2.0 Experimental Procedure

2.1 Sample Preparation

For this study, a commercially available polycrystalline disk superalloy Low-Solvus-High-Refractory (LSHR) and a single crystal Ni-base superalloy (SC-180) were tested. Table 1 compares the chemical compositions in weight percent of each alloy.

TABLE 1.—AVERAGE ALLOY COMPOSITION IN WEIGHT PERCENT

Alloy	Cr	Co	Al	Ti	Nb	Mo	Ta	W	Re	B	C	Ni
LSHR	12.5	20.4	3.5	3.5	1.5	2.7	1.5	4.3	0.0	0.03	0.045	Bal
SC-180	5	10	5.2	1.0	0.0	2.0	8.5	5.0	3.0	0.02	0.05	Bal

Before the two superalloys were joined, each alloy underwent separate heat treatments to acquire an optimized γ/γ' microstructure. For the polycrystalline disk alloy, LSHR, baseline samples were solution heat treated at 1171 °C for 2 h to produce a supersolvus microstructure and cooled at a rate of 72 °C per minute. This was followed by a two-step aging heat treatment beginning at 855 °C for 4 h proceeded by 775 °C for 8 h. These supersolvus “coarse grain” specimens had a mean linear intercept grain size of 15 μm . The effects that LSHR grain size has on residual stresses were explored in section 3.3 using supersolvus “fine grain” LSHR specimens, which had been solution heat treated at a lower temperature of 1135 °C before the same two-step aging heat treatment to give a mean linear intercept grain size of 8 μm . SC-180 was solution and aging heat treated according to U. S. Patent 4,935,072 (Ref. 23). Two different sized weld specimens were produced using electrical discharge machining for linear friction weld trials performed at Manufacturing Technology Inc. Figure 1 displays a schematic of the weld specimen sizes and set-up.

The SC-180 specimens were machined to align the [001] orientation with the transverse direction and [110] orientations with the longitudinal and normal directions, in both cases within a tolerance of 8°. Each weld analyzed for this study was created using the same LFW parameters.

Uniaxial tensile stress relaxation tests were performed for 24 h at 855 °C and then 775 °C on specimens having a nominal gage diameter of 0.41 cm and gage length of 2.1 cm, in a mechanical testing machine having a resistance heating furnace and axial extensometer. The tests were initiated at a strain rate of 0.5 percent per minute, in general accordance with the elevated temperature tensile testing specification ASTM E21-09. Each test was interrupted at a strain of 1 percent and held there for 24 h to measure relaxation of stress as a function of time at the constant imposed strain of 1 percent.

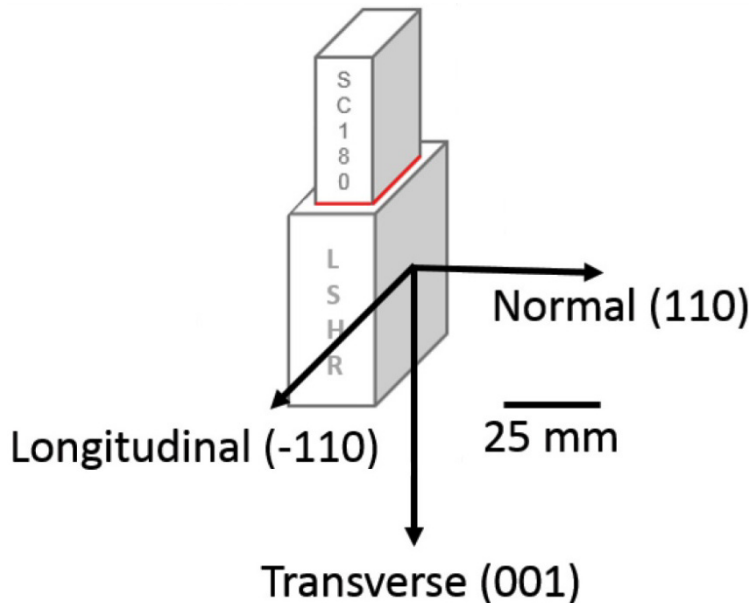


Figure 1.—A schematic revealing the size and welding process used to connect the polycrystalline LSHR to the single crystal SC-180. The linear friction weld oscillated along the longitudinal axis and the forge force was applied along the transverse axis. The arrows indicated the coordinates as well as the single crystal plane orientations of SC-180.

2.2 Measuring Residual Stress Using Neutron Diffraction

Following the weld trials, samples were sent to Oak Ridge National Laboratory to measure the residual lattice strain using the neutron diffractometer VULCAN at the Spallation Neutron Source (Ref. 24). A $2 \times 2 \times 2$ mm³ was used for the residual stress mapping. Using VDRIVE, a data reduction software produced by ORNL, lattice d-spacings were determined from neutron diffraction peak positions (Ref. 15). In measurements near the weld joint, peaks from the adjacent material could result in lower quality peak fits, adding error to the d-spacing measurements. This error was associated with higher χ^2 values. To mitigate this error, every d-spacing determination which corresponded to a χ^2 fit above 4 was re-examined and re-analyzed to account for the added peaks. An example of this analysis fix is shown in Figure 2.

The software also provides a d-spacing error associated with the quality of the fit. This error was propagated throughout the stress calculation and is displayed in the stress line graphs provided in the results section. Using the measured lattice d-spacing throughout the weld specimen, residual lattice strain can be calculated using Equation (1).

$$\varepsilon = \frac{d_{hkl} - d0_{hkl}}{d0_{hkl}} \quad (1)$$

Where d_{hkl} is the d-spacing of the lattice post weld, $d0_{hkl}$ is the d-spacing of the stress-free sample, and ε is the calculated lattice strain. $d0_{hkl}$ values were acquired using two methods: the first was to use the measured lattice spacing farthest from the weld as the stress-free value for both superalloys. The second, and more robust technique, was to produce two equivalent weld specimens and machine grids into one to relieve all the residual stress in macro scale. Thus, d-spacings could be compared between both samples from the same corresponding regions, where the gridded specimen provided $d0_{hkl}$ values and the intact specimen gave the d_{hkl} values. Using this approach allows the analysis to consider the chemical and structural changes which assuredly manifested near the weld joint, providing a more accurate representation of the residual stresses in the heat affected zones (HAZ) for both samples. This point-to-point stress free $d0$ selection will also minimize the strain artifact by edge effect as a result of partial material volume in the gauge volume near the short single-crystal-to-polycrystal interphase region.

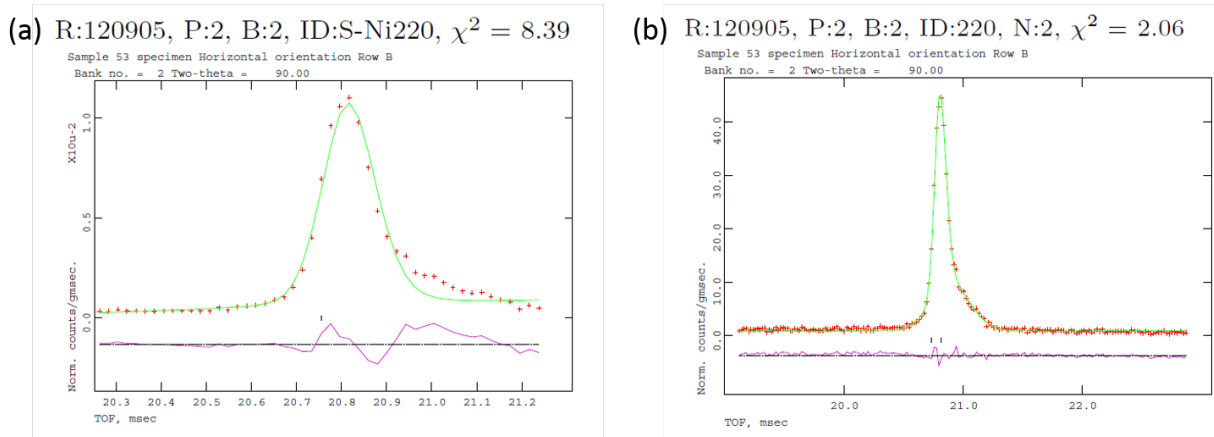


Figure 2.—An example of peak fitting that was determined to be (a) unacceptable and (b) satisfactory for determining the measured d-spacing of the sample region.

To measure the residual strain in the polycrystalline LSHR sample, the FCC (311) diffraction peak was used. From the lattice strain measurements residual stress could then be calculated. Since LSHR is polycrystalline in nature, the measured residual stress calculations could assume isotropic material properties. Therefore, the Hooks' law in Equation (2) was used to calculate the residual stress in all three directions orthogonal to the weld joint (transverse, longitudinal, and normal).

$$\begin{bmatrix} \varepsilon_{11} \\ \varepsilon_{22} \\ \varepsilon_{33} \end{bmatrix} = \frac{1}{E} \begin{bmatrix} 1 & -\nu & -\nu \\ -\nu & 1 & -\nu \\ -\nu & -\nu & 1 \end{bmatrix} \begin{bmatrix} \sigma_{11} \\ \sigma_{22} \\ \sigma_{33} \end{bmatrix} \quad (2)$$

Equation (2) displays the relationship between residual strain and stress where the diffraction elastic modulus of FCC (311) was experimentally measured to be $E_{311} = 217,219$ MPa and the corresponding Poisson's ratio to be $\nu_{311} = 0.292$ in LSHR.

For the single crystal SC-180 superalloy, symmetry of the FCC crystal structure allows for orthotropic material properties to be assumed. Thus, Equation (3) was used to measure residual stress in the transverse (1), longitudinal (2), and normal (3) directions.

$$\begin{bmatrix} \varepsilon_{11} \\ \varepsilon_{22} \\ \varepsilon_{33} \end{bmatrix} = \begin{bmatrix} \frac{1}{E_1} & -\frac{\nu_{21}}{E_2} & -\frac{\nu_{31}}{E_3} \\ -\frac{\nu_{12}}{E_1} & \frac{1}{E_2} & -\frac{\nu_{32}}{E_3} \\ -\frac{\nu_{13}}{E_1} & -\frac{\nu_{23}}{E_2} & \frac{1}{E_3} \end{bmatrix} \begin{bmatrix} \sigma_{11} \\ \sigma_{22} \\ \sigma_{33} \end{bmatrix} \quad (3)$$

Assuming orthotropic properties meant that the elastic modulus and Poisson's ratio needed to be measured for all three directions in the single crystal. The measured values are presented below in Table 2, except for $\nu[110][1-10]$, which was acquired by Sieborger et al. (Ref. 23).

In addition, a small rotation usually existed between the orientation of the single crystal and the weld directions being measured. For example, the [001] orientation of SC-180 was usually a few degrees off the transverse direction of the weld. This rotation was measured and considered in the final residual stress values. The software MATLAB (The MathWorks, Inc.) (Ref. 26) was used to perform the residual stress calculations as well as produce contour plots of the residual stress in the varying weld specimens, while Microsoft Excel was used to create the line graphs.

TABLE 2.—MEASURED MATERIAL PROPERTIES FOR SC-180

$E_1, [001]$	130629.54 MPa
$E_2 = E_3, [110]$	237337.35 MPa
$\nu_{12} = \nu_{13}, [001][110]$	0.389
$\nu_{32} = \nu_{23}, [110][1-10]$	-0.123 (Ref. 25)
$\nu_{21} = \nu_{31}, [110][001]$	0.694

3.0 Results

3.1 Effect of Sample Thickness on Residual Stress

The first residual stress measurements were performed to explore the effect different sized weld coupons had on residual stress profiles both near the weld joint and throughout the bulk specimens. For this study the strain free lattice measurements (d_{0hkl}) were taken at the far end of both samples, away from the weld joint. The schematic in Figure 3 describes the weld set up and size differences, which match those provided in Figure 1, between two microstructurally identical LSHR samples. The edge effect is not considered here for the grain size effect in the polycrystal samples, where coarse grain is much smaller than the gauge volume.

The residual stress was measured from the far end of the large specimen, taken in the center of the sample volume, across the weld joint and through to the other edge of the thin LSHR sample. In Figure 4, the calculated residual stress in all three directions (transverse, normal, and longitudinal) are plotted.

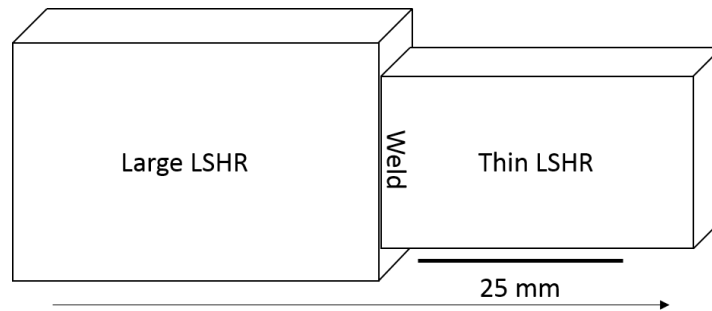


Figure 3.—A schematic showing the scan used to measure d -spacing across the weld joint of two different sized LSHR samples. The farther point from the weld in the smaller LSHR sample was used for an assumed d_{0hkl} value.

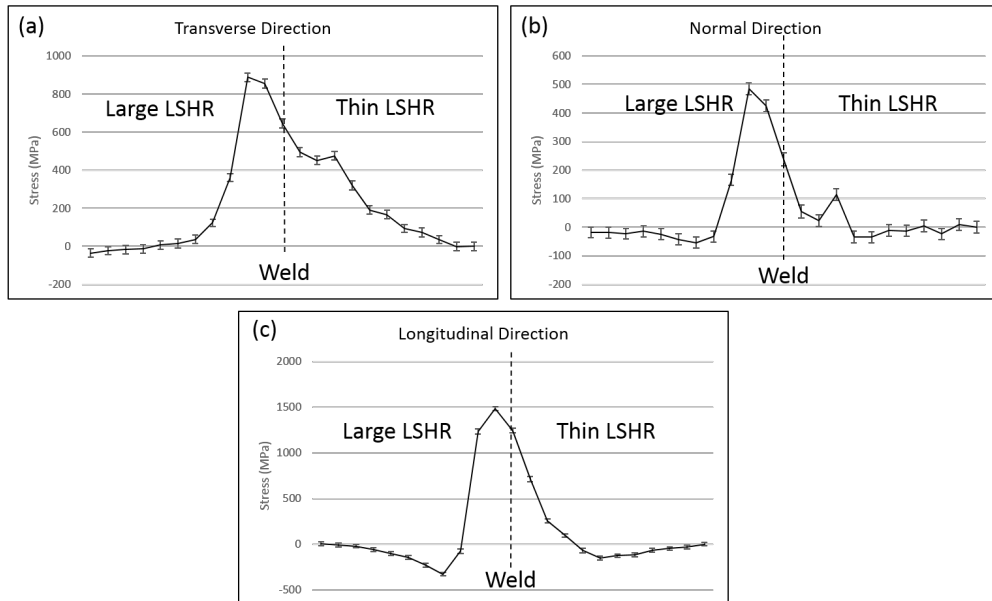


Figure 4.—The residual stress measured in the (a) transverse direction, (b) normal direction, and (c) longitudinal direction across the weld starting from the edge of the larger LSHR sample to the other edge of the smaller LSHR sample. Each measurement was taken in 2 mm increments across the weld joint.

Figure 4 reveals the highest residual stress in the polycrystalline LSHR to polycrystalline LSHR weld occurs in the longitudinal direction, the same direction the samples were oscillated during the LFW. Significant stresses are also observed in the transverse direction, the same direction the samples were forged during and after the weld. The lowest residual stress measurements were seen in the normal direction of the weld. Though the stresses were higher in the thick LSHR sample, they did not extend as far into the sample as compared to the smaller LSHR sample.

3.2 Effect of Post-Weld HIP Cycles on Residual Stress

Following the study on thickness effects, which used LSHR for both specimen, the rest of the work presented uses a large LSHR sample welded to a smaller SC-180 single crystal. To relieve the residual stresses observed in the as-welded condition of the polycrystalline to single crystal welds, two identical samples were HIPed while repeating the two-step aging heat treatment originally applied to LSHR. After the HIP cycle, in order to provide unstrained lattice d-spacing values, grids were wire electro discharge machined into the surface of one sample thus relieving its residual stress. A schematic of the regions examined using neutron diffraction is shown in Figure 5.

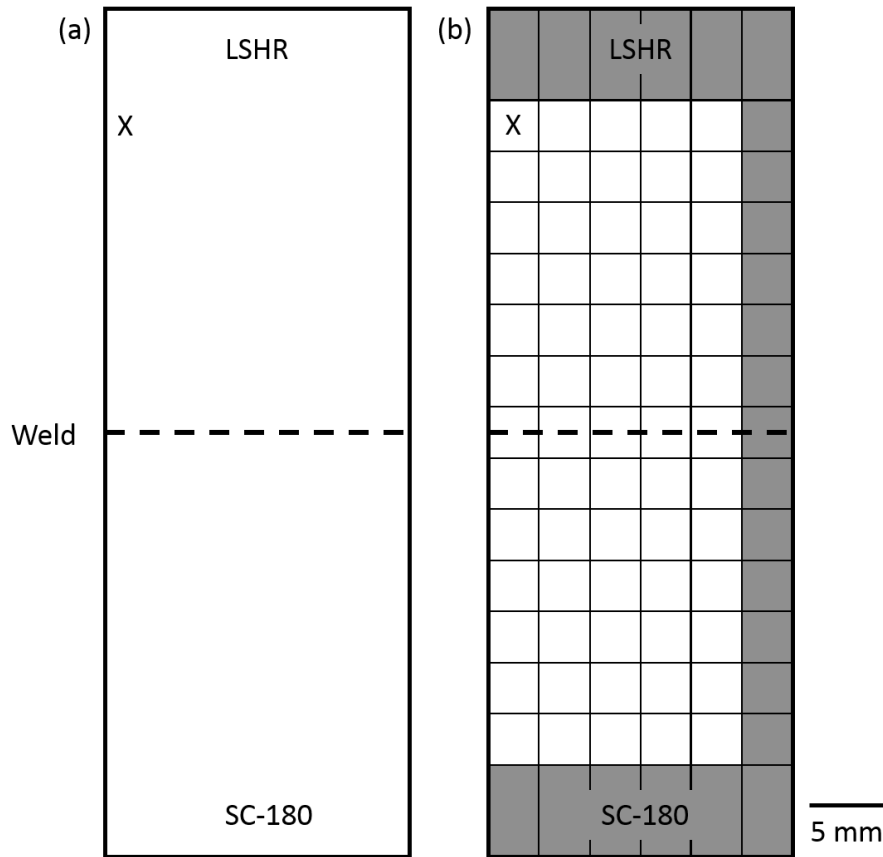


Figure 5.—Schematic of how the 2-d contour plots were produced. Two identical weld samples were produced so that d-spacings could be measured (a) in the as-welded condition and (b) in a sample that was gridded to relax the residual stress. This latter sample would be used for reference d_{0hkl} values while the intact condition would be used for d_{hkl} values. The shaded regions denote areas that were not measured. The X marks an example of where/how the measurements were compared.

In Figure 5, two identical LFW samples were produced. One sample Figure 5(a) was kept intact while the other sample Figure 5(b) had grids machined into it. The lattice spacing for corresponding areas were compared. For example, the regions denoted by an “X” in Figure 5 were compared to determine residual stress. The grids shaded in gray correspond to areas that were not examined using neutron diffraction due to time constraints. In Figure 6, contour plots presenting the residual stress layout in all three directions described in Figure 1 are shown for the as-welded condition.

The highest residual stresses are observed along the weld joint in the longitudinal direction. This same observation was presented for the LSHR to LSHR weld shown in Figure 4. The residual stress profile in the transverse direction presents a large tensile stress on the left side of the joint next to a compressive residual stress on the right. Compressive stresses are also observed in the normal direction about a centimeter away from the weld joint in the normal direction for both alloys. Figure 7 shows the stress profiles after the weld specimen undergoes a HIP cycle.

A significant reduction in the residual stress profile can be observed in all three directions along the weld joint after the HIP cycle. However, there is a notable increase in the compressive residual stresses in the longitudinal direction throughout much of the SC-180 sample. For a better comparison between the stress levels in the as-welded and post-HIP samples, Figure 8 compares the line profiles taken from the center column of grids in both samples.

In all three directions the residual stress on or near the weld was significantly reduced after the post-weld HIP cycle. A notable reduction in the transverse and longitudinal tensile stresses in SC-180 is shown in Figure 8(a) and (c), respectively. However, the reduction on the LSHR side of the weld joint was found to be much less pronounced.

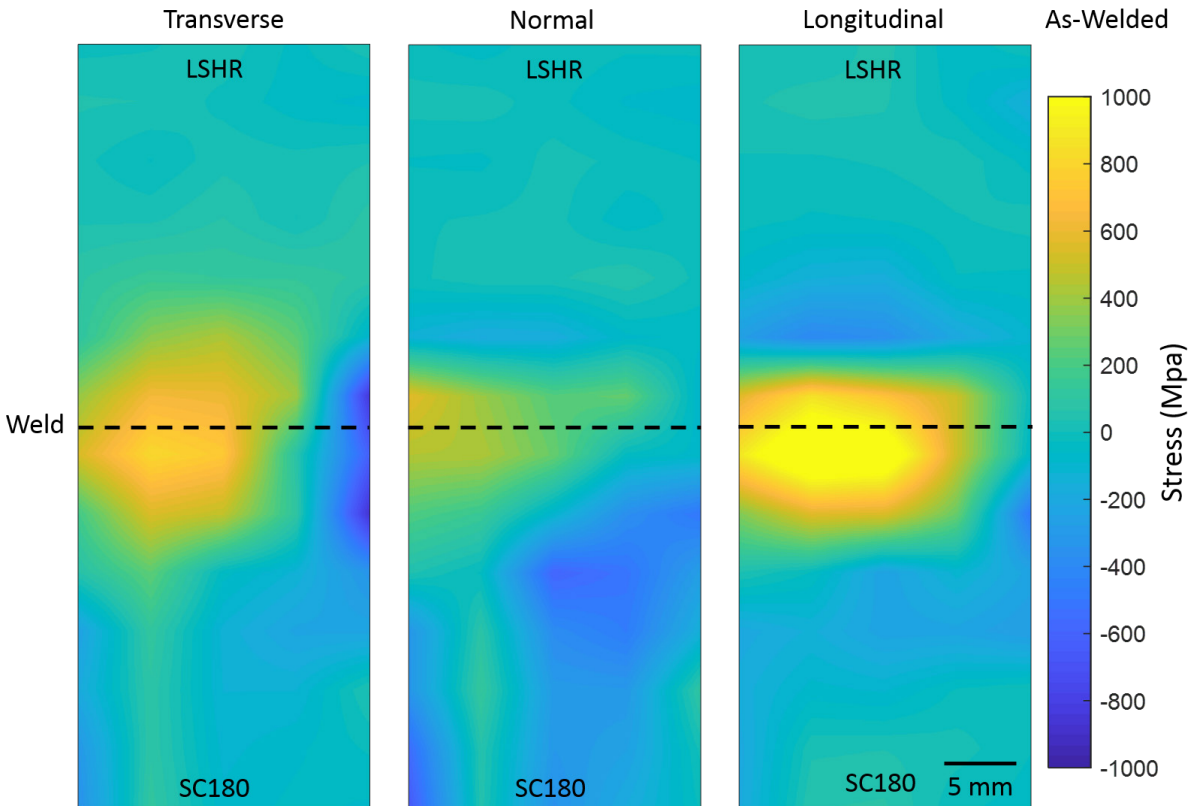


Figure 6.—Two-dimensional contour plots of the residual stress in the transverse, normal, and longitudinal directions of a sample in the as-welded condition. Note: the excluded areas are not represented in the contour plot.

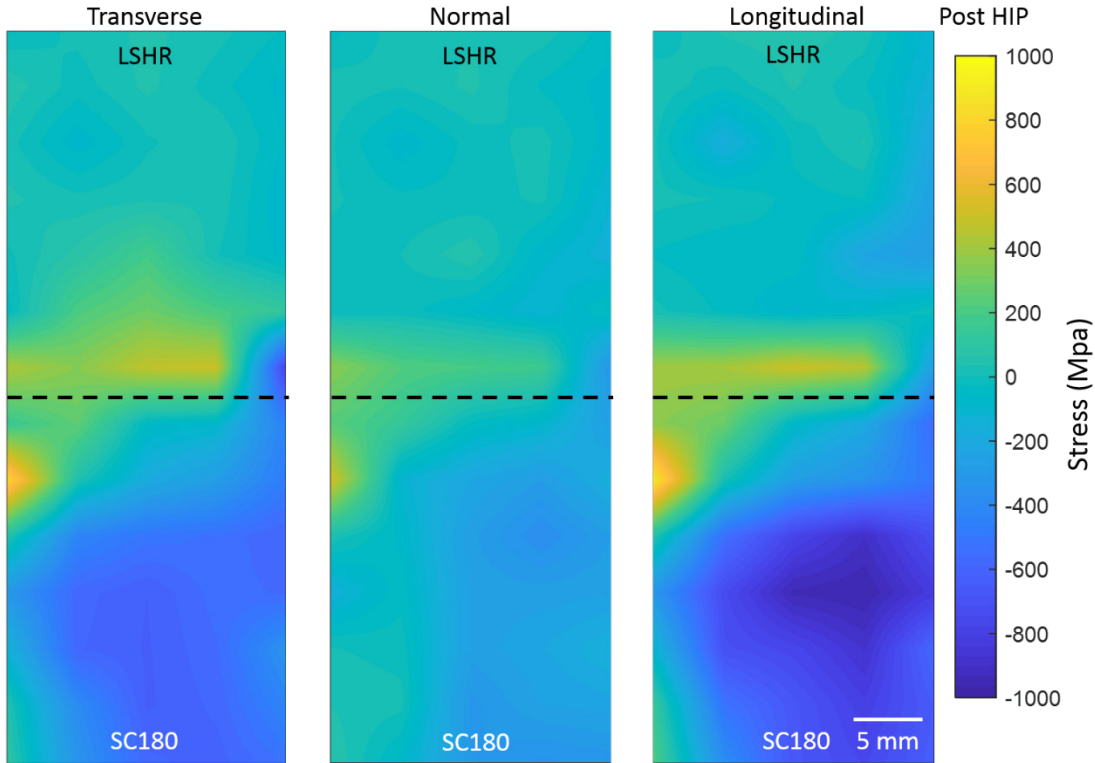


Figure 7.—Two-dimensional contour plots of the residual stress in the transverse, normal, and longitudinal directions of a sample after a post-weld HIP cycle.

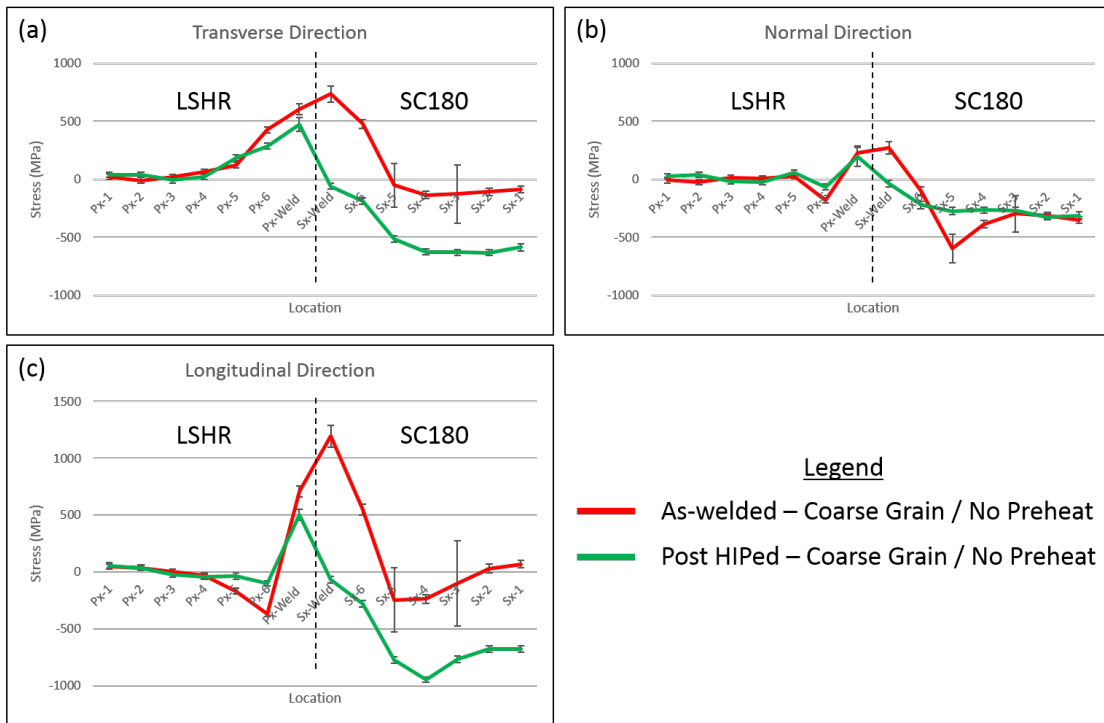


Figure 8.—The residual stress measurements comparing the as-welded and post-HIP conditions in the (a) transverse direction, (b) normal direction, and (c) longitudinal direction. The graphs reflect the measurements taken from the center of the two-dimensional contour plots revealed in Figure 6 and Figure 7. The dashed line represents where the weld is located on each graph.

3.3 Effect of Pre-Heat on Residual Stress

Another approach explored in this study was the effect pre-heat temperatures prior to welding had on residual stresses. In addition, the difference LSHR grain size had on residual stress was explored. Again, two identical samples for each condition were produced, where one had grids cut into it to relieve the stress and provide strain free lattice measurements. Figure 9 shows the area that was measured using neutron diffraction for this study.

Two different pre-heat conditions were explored 315 °C (600 °F) and 540 °C (1000 °F). Figure 10 reveals the transverse residual stress measurements for all four conditions explored.

Notable differences in the measured residual stresses were found along the weld joint, corresponding to different pre-heat temperatures. Both the coarse and fine grain LSHR specimens pre-heated to 540 °C displayed a significant reduction in post-weld residual stress, followed by the 315 °C pre-heat condition which still gave a notable stress reduction when compared to the no pre-heat weld specimen. Figure 11 reveals the normal stress for all four conditions.

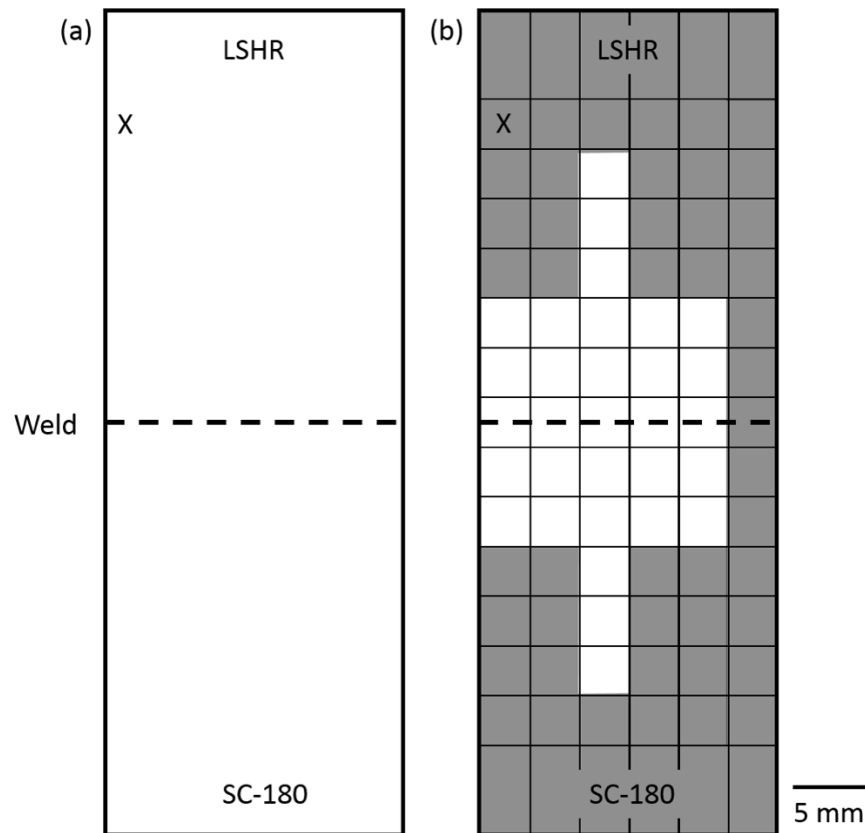


Figure 9.—Schematic of how the two-dimensional contour plots were produced. Two identical weld samples were produced so that d-spacings could be measured (a) in the as-welded condition after a certain weld pre-heat and (b) in a sample that was gridded to relax the residual stress. This latter sample would be used for reference d_{0hkl} values while the intact condition would be used for d_{hkl} values. The shaded regions denote areas that were not measured. The X marks an example of where/how the measurements were compared.

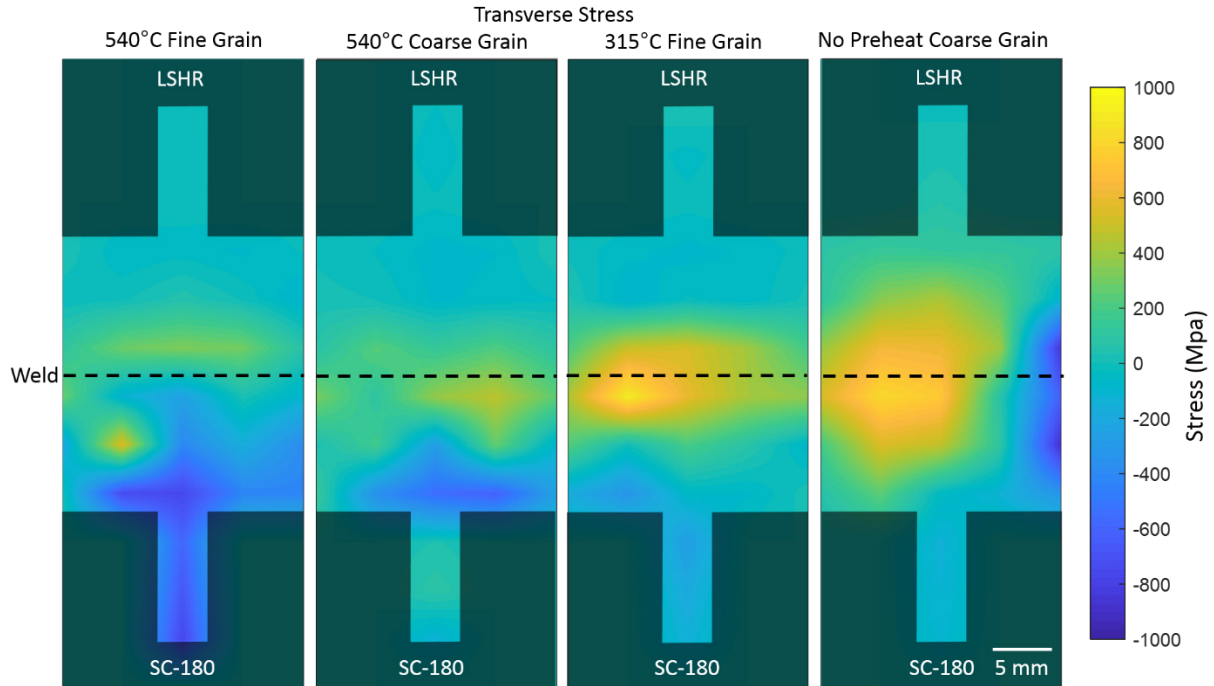


Figure 10.—Two-dimensional contour plots of the residual stress in the transverse direction after 540 °C pre-heat and fine grained LSHR, 540 °C pre-heat and coarse grained LSHR, 315 °C pre-heat and fine grained LSHR and no pre-heat and coarse grained LSHR.

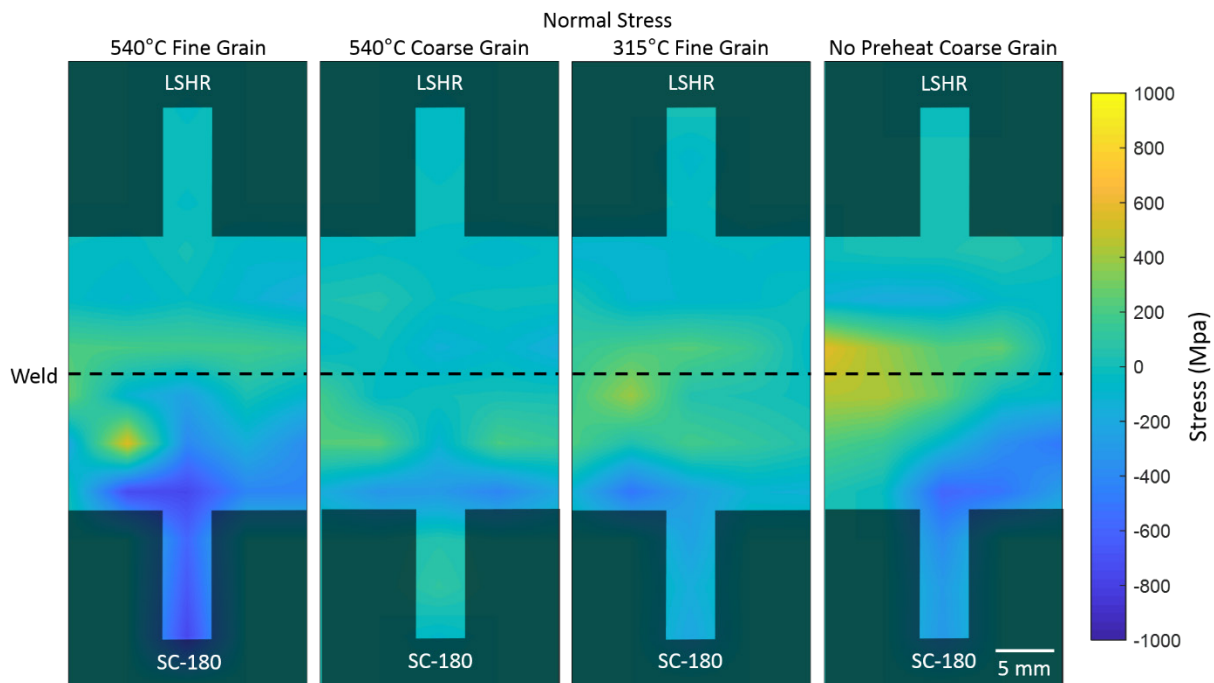


Figure 11.—Two-dimensional contour plots of the residual stress in the normal direction after 540 °C pre-heat and fine grained LSHR, 540 °C pre-heat and coarse grained LSHR, 315 °C pre-heat and fine grained LSHR, and no pre-heat and coarse grained LSHR.

Many of the same trends observed in the transverse direction can be seen with the normal direction stress measurements. However, there does appear to be a slight improvement in stress levels along the weld joint for the sample pre-heated to 540 °C with the coarse grain LSHR over the fine grain LSHR. The residual stress measurements in the longitudinal direction are displayed in Figure 12.

As was determined in Sections 3.1 and 3.2, the longitudinal stresses were found to be the highest for all four pre-heat conditions. Additionally, the higher pre-heat weld specimens displayed marked improvements in residual stress, with the no pre-heat sample presenting the highest residual stress values. Interestingly, the 540 °C pre-heat samples exhibited higher compressive longitudinal stress values in the bulk of SC-180 as well. In order to better visualize the measured variations in stress between the different pre-heat and grain size conditions, the residual stress taken from the center of the two-dimensional contour plots revealed in Figure 10 to Figure 12 are plotted against each other in Figure 13.

Regarding stress at or near the weld joint, the higher pre-heat specimens presented the greatest decrease as compared to the no pre-heat sample. This finding has also been observed for arc-welded steel (Ref. 27)[27]. Although it is difficult denoting a significant difference between the coarse and fine grain samples with a preheat of 540 °C, the coarse grain samples did consistently result in smaller stress values near the weld joint for LSHR. In addition, the fine grain LSHR specimens appear to have produced larger compressive stresses in the bulk single crystal specimens for all three directions. Still, as was found after the HIP cycle, the pre-heat temperature and LSHR grain size appear to affect the residual stresses in the SC-180 single crystal much more than in the polycrystalline LSHR samples.

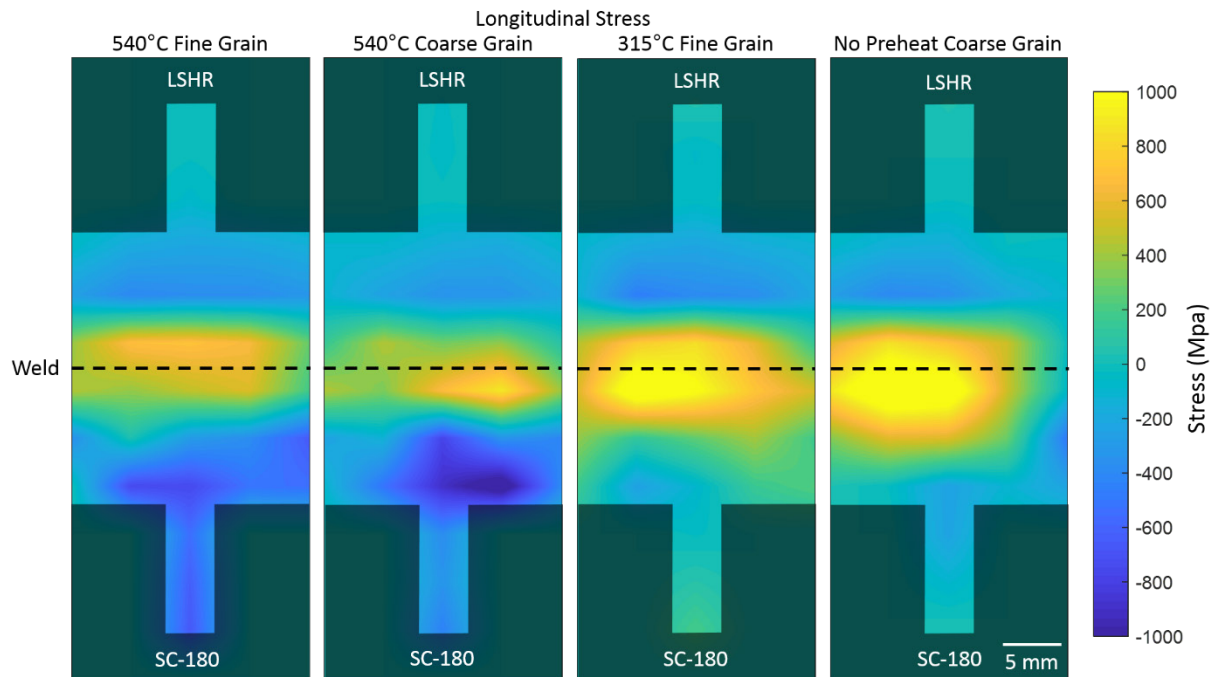


Figure 12.—Two-dimensional contour plots of the residual stress in the longitudinal direction after 540 °C pre-heat and fine grained LSHR, 540 °C pre-heat and coarse grained LSHR, 315 °C pre-heat and fine grained LSHR, and no pre-heat and coarse grained LSHR.

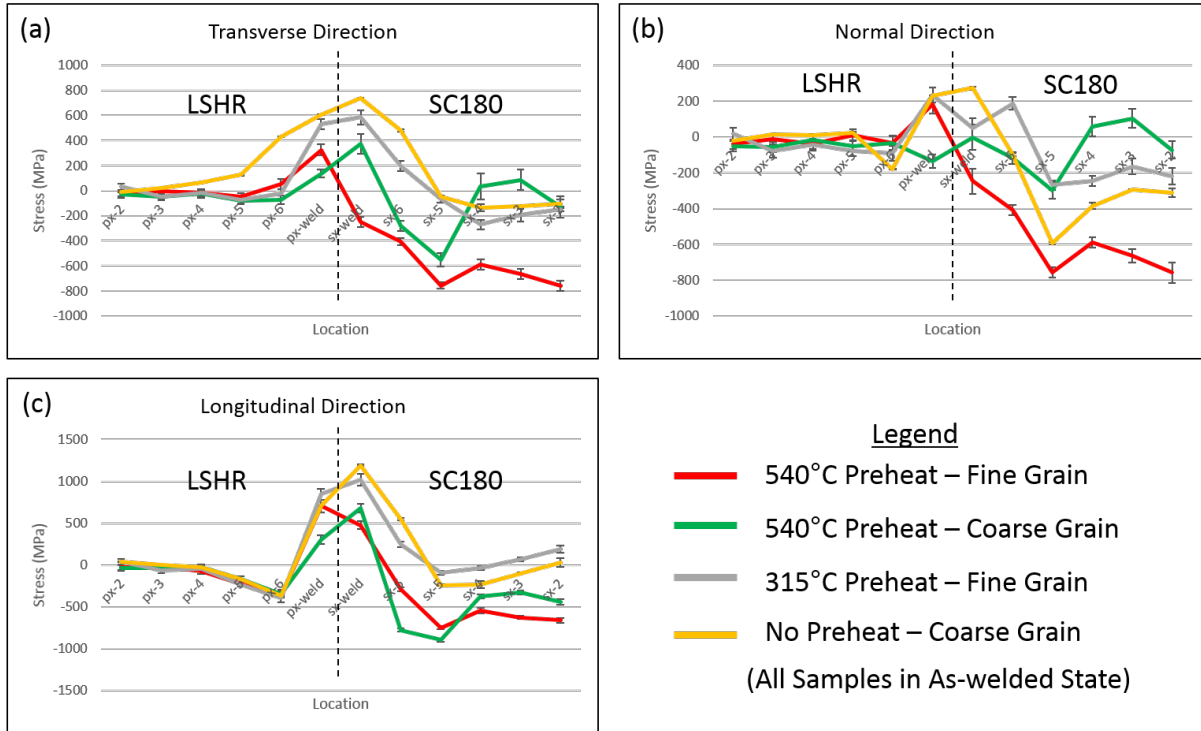


Figure 13.—The residual stress measurements comparing the different pre-heat and grain size effects on residual stress taken from the center of the Two-dimensional contour plots revealed in Figure 10 to Figure 12 for the (a) transverse direction, (b) normal direction, and (c) longitudinal direction. The dashed line represents where the weld is located on each graph.

4.0 Discussion

4.1 Microstructural Characterization of Weld Joints

Microstructural characterization of the weld joints was performed using scanning electron microscopy (SEM) to explore the effect LSHR grain size had on the materials response near the weld joint. In both welds, a 315 °C pre-heat was employed prior to the weld. Backscatter Electron (BSE) images acquired using a Hitachi S4700 II of the fine grain LSHR sample are shown in Figure 14 (Ref. 28).

The BSE images shown in Figure 14(a) and (b) reveal that LSHR grain size actually increased in the material approaching the weld joint. The higher temperatures appear to have promoted grain growth during the LFW (Ref. 29). In Figure 15, the same analysis is displayed for the coarse grain LSHR specimen.

Surprisingly, the coarse grain LSHR exhibited the opposite microstructural evolution response during the LFW. Instead of the grains coarsening near the weld interface they became significantly finer. The deformation induced during the welding and the high temperatures appears to generate dynamic recrystallization in the HAZ areas near the weld. The ability of the microstructure to recrystallize in the coarse grain LSHR may explain the lower residual stresses observed near the weld joints as compared to the fine grain LSHR welds. In fact, recrystallization is a known process that relieves residual stress in highly strained microstructures (Ref. 30). Previously, a study by Iqbal et al. (Ref. 31) also explored the effect grain size had on residual stress in another disk superalloy RR1000 after inertia welding and could not find a significant difference between stress values and pre-weld grain sizes. However, their study only explored polycrystalline to polycrystalline welds which may have contributed to the discrepancy between their results and those found in this study. Still, their findings indicate that the coarse grain material recrystallized in the HAZ near the weld joint, which was also observed in this study.

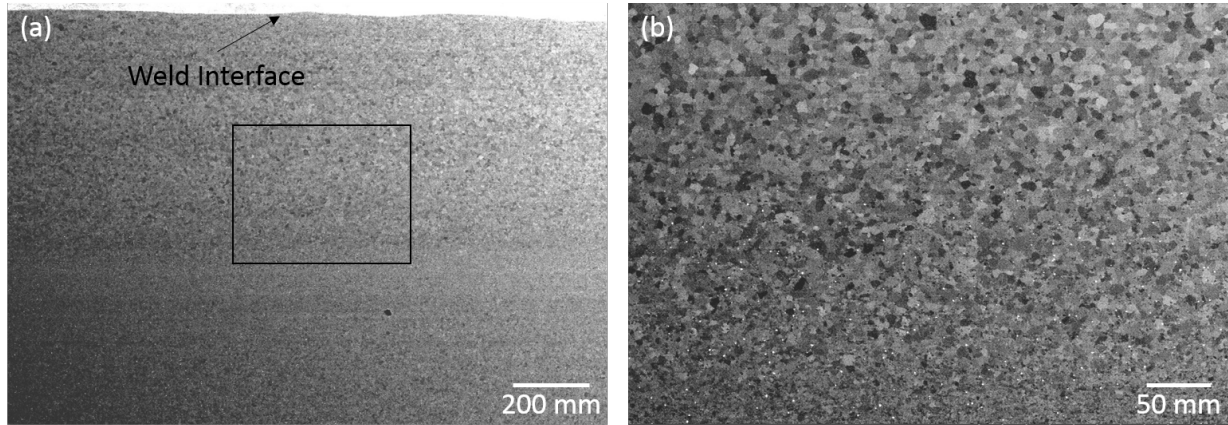


Figure 14.—SEM BSE images revealing the microstructural changes that occurred in the fine grain LSHR at (a) and (b) high magnifications. The block box in (a) corresponds to the image shown in (b).

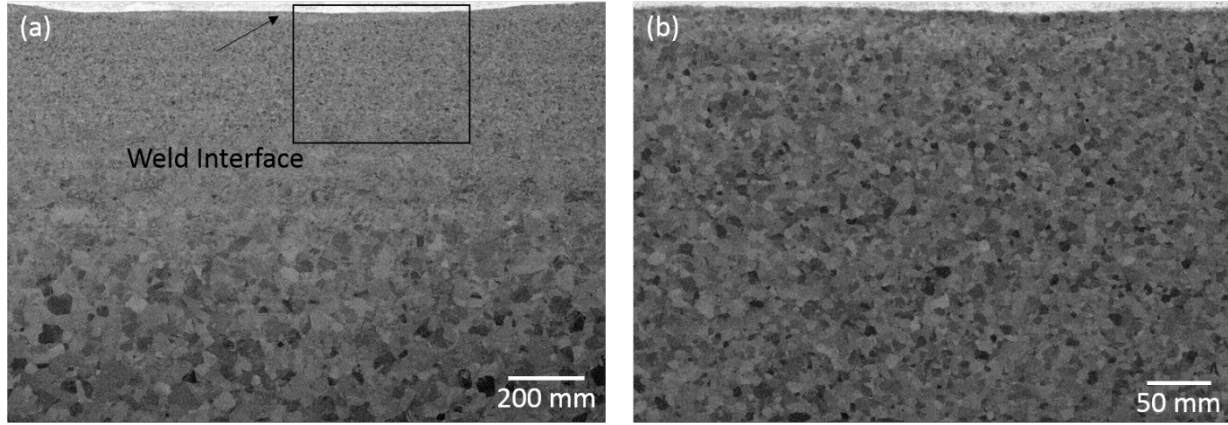


Figure 15.—SEM BSE images revealing the microstructural changes that occurred in the coarse grain LSHR at (a) and (b) high magnifications. The block box in (a) corresponds to the image shown in (b).

The HIP cycle was intended to allow relaxation of residual stresses near the joint. After recrystallization, the finer grain size near the joint could allow more relaxation of residual stresses during this HIP cycle. In order to assess the effect of such changing grain size in LSHR on the subsequent relaxation of residual stresses near the weld joint during the HIP cycle, uniaxial tensile stress relaxation tests were performed on fully heat treated LSHR materials having purposefully varied grains sizes “coarse grain” (15 μm) and “fine grain” (8 μm). The relaxation tests were also performed on single crystal SC-180, as another basis of comparison. As shown in Figure 16, it is clear that the LSHR undergoes more relaxation of stress than SC-180 at each temperature. Furthermore, residual stress in the fine grain LSHR specimen appears to relax more than in the coarse grain LSHR. This can help explain why the fine grains produced by recrystallization near the joint could result in lower measured residual stresses.

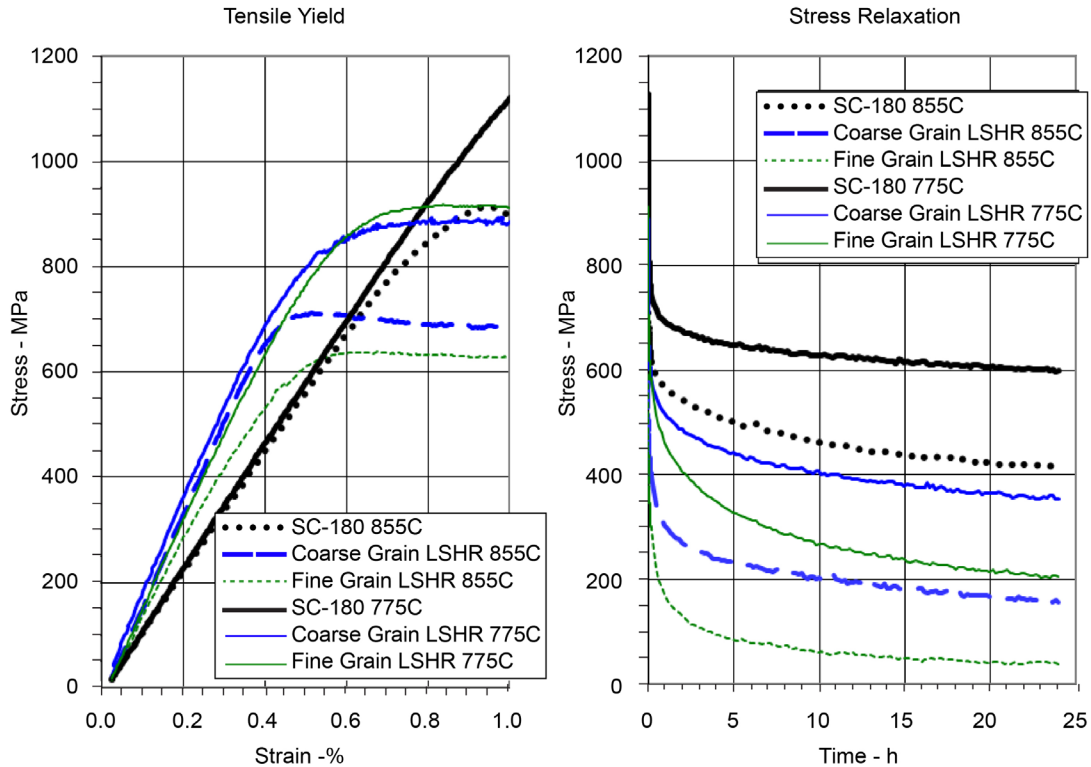


Figure 16.—Comparison of tensile yield and stress relaxation responses in uniaxial stress relaxation tests of single crystal SC-180, coarse grain LSHR, and fine grain LSHR at 855 and 775 °C.

4.2 Effect Pre-Heating has on Overall LFW Temperatures

In Section 3.3, it was discovered that higher pre-heat temperatures before performing LFWs resulted in lower residual stresses. To better understand the effect that different preheat temperatures have on the sample microstructures and LFW process, Inconel sheathed thermocouples were placed in machined holes within both LSHR and SC-180. In the SC-180 sample, the thermocouple was placed 1.3 mm away from the weld interface. In contrast, since most of the deformation occurs in LSHR during the LFW, the LSHR thermocouples were positioned 3.3 mm away from the interface as they would not survive if placed closer. Four different pre-heat temperatures were used in this study: 315, 427, 482, and 540 °C. In Figure 17, the measured temperature profiles from the SC-180 sample using different pre-heat weld trials are shown.

Although the highest pre-heat temperature did result in the highest measured weld temperatures, the trend did not extend to the other three pre-heat temperatures. In fact, the lowest weld temperature corresponded with the second highest pre-heat temperature (482 °C). However, the correlation between weld temperature and pre-heat temperature does appear stronger in LSHR as shown in Figure 18.

In LSHR, there does appear to be a correlation between pre-heat temperatures and weld temperature, where the higher pre-heat temperatures resulted in higher weld temperatures. Still, the trend is not met for all cases as shown by the temperature profiles of the 427 °C and 482 °C pre heat conditions. This observation may show that though pre-heating before the weld can have an effect on the overall temperatures experienced by the two samples during the weld, other factors also play a role. At the moment it is not clear what other weld parameters or microstructure characteristics may affect weld temperatures or if there is significant temperature variation from weld to weld even though all weld parameters remained consistent.

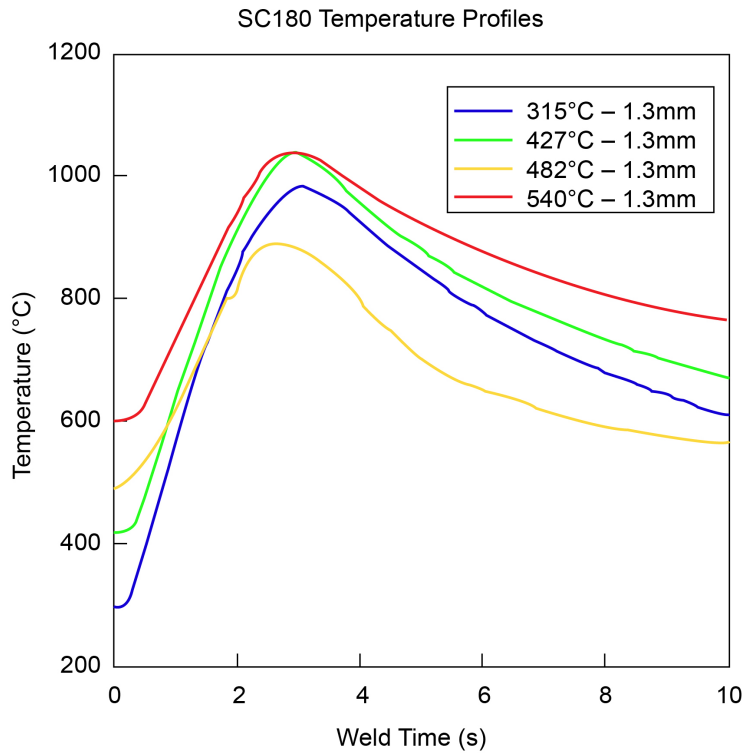


Figure 17.—Comparison between the measured temperature profiles during LFWs in SC-180 when different pre-heat temperatures are employed. Thermocouples were placed 1.3 mm from the weld interface.

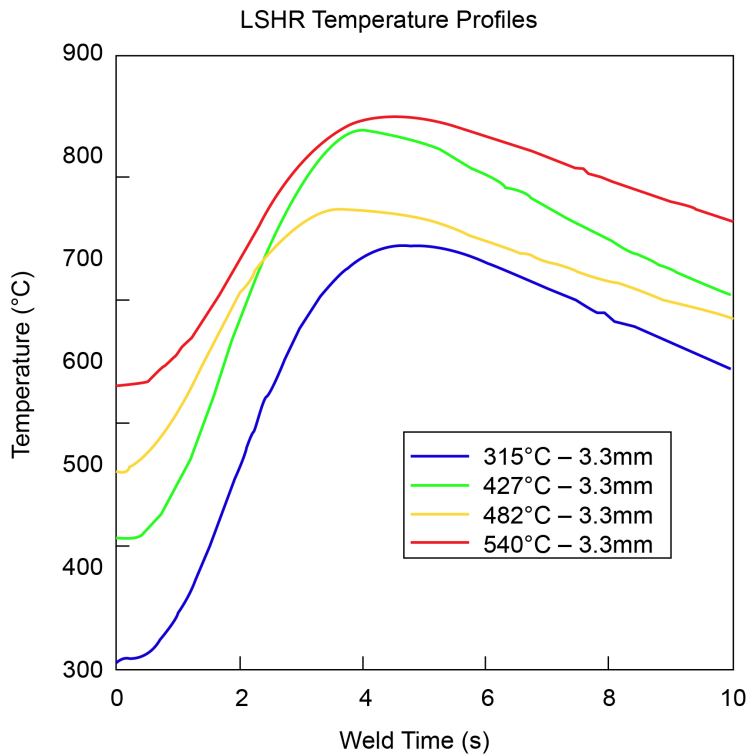


Figure 18.—Comparison between the measured temperature profiles during LFWs in LSHR when different preheat temperatures are employed. Thermocouples were placed 3.3 mm from the weld interface.

4.3 Residual Stress Measurements by Contour Method

To compare the conclusions drawn from the neutron diffraction results, new residual stress measurements were obtained using an alternative method. Two identical weld specimens of coarse grain LSHR and SC-180 using the same parameters described in the methods section and employing the 315 °C pre-heat were produced. After welding, one specimen was kept in the as-welded state while the other was HIPed as described before. These specimens were then sent to Hill Engineering which utilized the contour method to measure residual stresses (Refs. 32 and 33). Each specimen was sectioned to measure the residual stresses normal to the cut plane and received two contour measurements for a total of twelve planes. The first cut was oriented to measure the residual stress in the longitudinal weld direction while the second cut occurred along the weld following longitudinal stress measurement. The proximity and intersection of the first contour measurement plane with the second resulted in partial release of the residual stress on the second plane. The released stress at the subsequent plane was calculated as part of the initial measurement. Total stress at the second plane was calculated using elastic superposition as the sum of the released stress and the measured stress. The same material properties used to calculate residual stress using neutron diffraction were employed for this method as well. Figure 19 compares the longitudinal stress measured across the weld while still in the as-welded condition for both the contour method and neutron diffraction.

Figure 19 reveals the measured residual stress in the longitudinal direction at the center of the specimen using the contour method (red line) and neutron diffraction (blue squares). Both measurements reveal the same trend and comparable stress levels near the weld joint. The only exception was a slight difference in stresses measured in the single crystal. This may be explained by small differences in single crystal orientation between the two tests or normal variations experienced between each weld trial. In Figure 20, the residual stress measurements in the post-HIP sample are compared to the as-welded measurements.

As was confirmed in Figure 6 to Figure 8, the HIP cycle was successful in significantly lowering the residual stress near the weld joint. Indeed, Figure 20 presents similar results to the residual stresses presented in Figure 8(c) as well, revealing a comparable stress reduction to those measured using neutron diffraction.

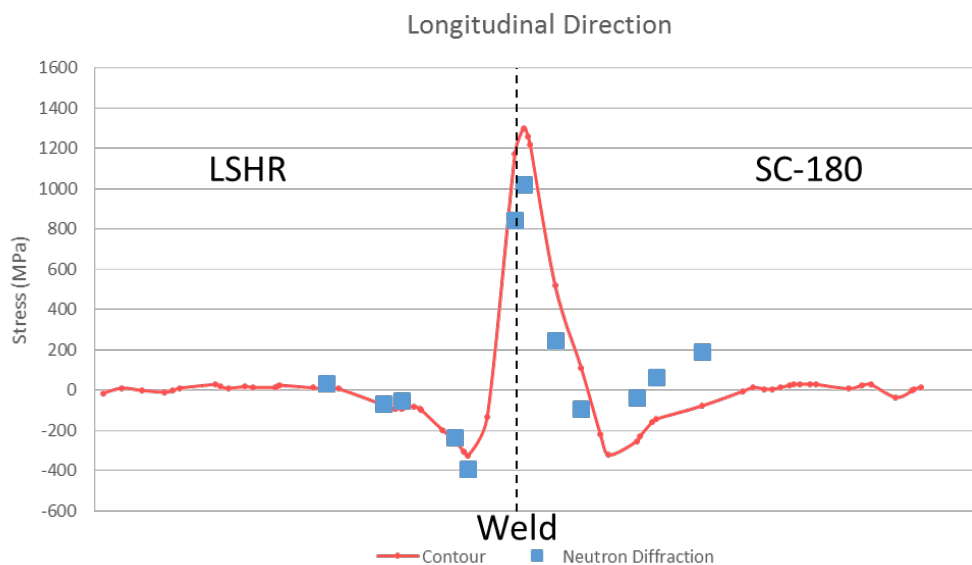


Figure 19.—Comparison between residual stress measurements using the contour method (red line) and neutron diffraction (blue squares).

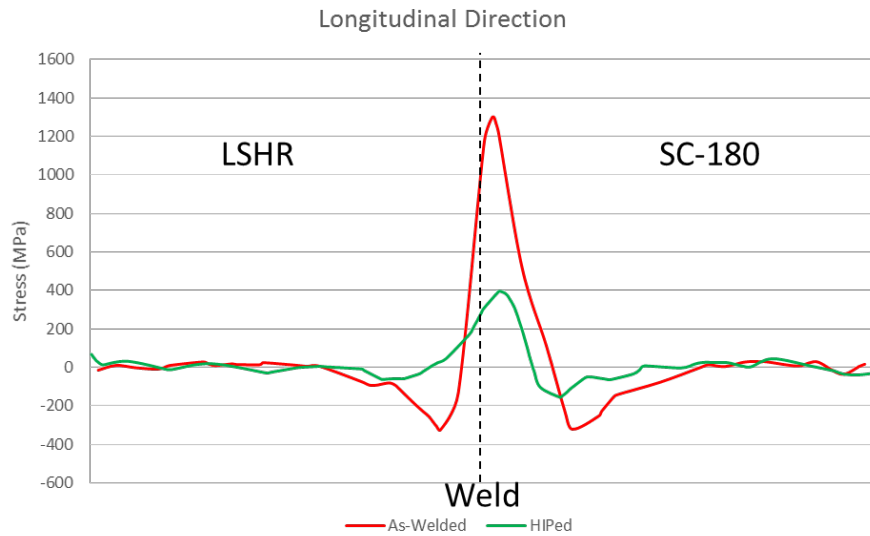


Figure 20.—Contour method residual stress measurements for as-welded and post HIP weld specimens which were preheated to 315 °C. The error associated with the data used for these curves is ± 29 MPa.

5.0 Conclusions

This study explored multiple avenues to lower the residual stresses produced when a polycrystalline disk alloy (LSHR) is joined to a single crystal superalloy (SC-180) using linear friction welding. From state-of-the-art neutron diffraction and microstructural characterization several notable conclusions can be drawn.

1. Sample size differences between the two weld specimens will produce different stress profiles throughout their respective microstructures. The larger samples contain higher residual stresses but dissipate the stress more quickly away from the weld interface. In the as-welded state, these residual stresses can reach levels near the ultimate tensile strength of LSHR.
2. Post-weld HIP cycles effectively lower the residual stresses, especially in the single crystal. The HIP cycle only provides a modest reduction in stress for the polycrystalline LSHR samples.
3. Pre-heating the weld specimens provides a significant reduction in post-weld residual stresses. The highest measured pre-heat temperatures give the greatest reduction in stress. Again, the largest residual stress reductions are observed in the single crystal.
4. Initial average grain size in the polycrystalline LSHR specimen results in different HAZ microstructural responses. The fine grain specimen experiences grain growth while the coarse grain sample exhibits grain recrystallization. This recrystallization may explain the lower residual stresses found in the coarse grain LSHR near the weld joint as compared to the fine grain LSHR samples.
5. Higher pre-heat temperatures appear to contribute to higher weld temperatures, though this trend is not always consistent, implying that other mechanisms may also contribute to overall LFW temperature profiles.
6. The residual stress values obtained through the contour method can be used to strengthen the conclusions acquired by the neutron diffraction analysis.

All these conclusions will help inform future LFW trials. From these results high pre-heat temperatures and post-weld HIP cycles are encouraged to lower the residual stresses that inherently manifest during the LFW process. In addition, coarser grain microstructures may help lower the residual stress in the polycrystalline sides of the weld joints by encouraging grain recrystallization.

References

1. E.M. Greitzer, P.A. Bonnefoy, E. De la Rosa Blanco, C.S. Dorbian, M. Dreila, D.K. Hall, R.J. Hansman, J.I. Hileman, R.H. Liebeck, J. Lovegren, P. Mody, J.A. Pertuze, S. Sato, Z.S. Spakovzky, T. C.S., N + 3 Aircraft Concept Designs and Trade Studies , Final Report: Volume 1, NASA Contract. Rep. VOL1 (2010).
2. R. Reed, *The Superalloys: Fundamental and Applications*, Cambridge University Press, New York, 2006.
3. T.M. Pollock, Alloy design for aircraft engines, *Nat. Publ. Gr.* 15 (2016) 809–815. <https://doi.org/10.1038/nmat4709>.
4. M. Karadge, M. Preuss, P.J. Withers, S. Bray, Importance of crystal orientation in linear friction joining of single crystal to polycrystalline nickel-based superalloys, *Mater. Sci. Eng. A.* 491 (2008) 446–453. <https://doi.org/10.1016/j.msea.2008.04.064>.
5. O.N. Senkov, D.W. Mahaffey, S.L.E.E. Semiatin, C. Woodward, Inertia Friction Welding of Dissimilar Superalloys Mar-M247 and LSHR, *Metall. Mater. Trans. A.* 45 (2014) 5545–5561. <https://doi.org/10.1007/s11661-014-2512-x>.
6. A. Chamanfar, M. Jahazi, J. Cormier, A Review on Inertia and Linear Friction Welding of Ni-Based Superalloys, *Metall. Mater. Trans. A.* 46 (2015) 1639–1669. <https://doi.org/10.1007/s11661-015-2752-4>.
7. J. Dahal, K. Maciejewski, H. Ghonem, Grain Boundary Deformation and Fracture Mechanisms in Dwell Fatigue Crack Growth in Turbine Disk Superalloy ME3, *Superalloys 2012 (12th Int. Symp. Superalloys)*. (2012) 149–158.
8. E.S. Huron, K.R. Bain, D.P. Mourer, J.J. Schirra, P.L. Reynolds, E.E. Montero, The Influence of Grain Boundary Elements on Properties and Microstructures of P/M Nickel Base Superalloys, *Superalloys 2004 (Tenth Int. Symp.)* (2004) 73–81. https://doi.org/10.7449/2004/Superalloys_2004_73_81.
9. H.L. Danflou, M. Marty, A. Walder, Formation of serrated grain boundaries and their effect on the mechanical properties in a P/M nickel base superalloy, *Superalloys 1992*. (1992) 63–72.
10. A. Soula, Y. Renollet, D. Boivin, J.L. Pouchou, D. Locq, P. Caron, Y. Bréchet, Grain Boundary and Intragranular Deformations During High Temperature Creep of a PM Nickel-Based Superalloy, *Superalloys 2008 (Eleventh Int. Symp.)* (2008) 387–394.
11. T. Osada, Y. Gu, N. Nagashima, Y. Yuan, T. Yokokawa, Optimum microstructure combination for maximizing tensile strength in a polycrystalline superalloy with a two-phase structure, *Acta Mater.* 61 (2013) 1820–1829. <https://doi.org/10.1016/j.actamat.2012.12.004>.
12. J. Gayda, T.P. Gabb, P.T. Kantzos, The Effect of Dual Microstructure heat Treatment on an Advanced Nickel-Base Disk Alloy, *Superalloys 2004*. (2004) 323–329.
13. J. Gayda, Dual Microstructure Heat Disk Alloy Treatment of a Nickel-Base, NASA/TM. 211168 (2001).
14. O.T. Ola, O.A. Ojo, P. Wanjara, M.C. Chaturvedi, A Study of Linear Friction Weld Microstructure in Single Crystal CMSX-486 Superalloy, *Metall. Mater. Trans. A.* 43 (2012) 921–933. <https://doi.org/10.1007/s11661-011-0928-0>.

15. K. An, VDRIVE Data Reduction and Interactive Visualization Software for Event, ORNL/TM/2012/621. (2012).
16. M.R. Daymond, N.W. Bonner, Measurement of strain in a titanium linear friction weld by neutron diffraction, *Phys. B.* 325 (2003) 130–137.
17. M. Smith, J. Levesque, L. Bichler, D. Sediako, J. Gholipour, P. Wanjara, *Materials Science & Engineering A Residual stress analysis in linear friction welded in-service Inconel 718 superalloy via neutron diffraction and contour method approaches*, *Mater. Sci. Eng. A.* 691 (2017) 168–179. <https://doi.org/10.1016/j.msea.2017.03.038>.
18. I. Bhamji, M. Preuss, P.L. Threadgill, R.J. Moat, A.C. Addison, M.J. Peel, Linear friction welding of AISI 316L stainless steel, *Mater. Sci. Eng. A.* 528 (2010) 680–690. <https://doi.org/10.1016/j.msea.2010.09.043>.
19. A.R. McAndrew, P.A. Colegrove, C. Bühr, B.C.D. Flipo, A literature review of Ti-6Al-4V linear friction welding, *Prog. Mater. Sci.* 92 (2018) 225–257. <https://doi.org/10.1016/j.pmatsci.2017.10.003>.
20. P.J. Withers, H.K.D.H. Bhadeshia, P.J. Withers, H.K.D.H. Bhadeshia, Residual stress. Part 1 – Measurement techniques Residual stress Part 1 – Measurement techniques, *Mater. Sci. Technol.* 17 (2001) 355–365. <https://doi.org/10.1179/026708301101509980>.
21. M. Preuss, J.W.L. Pang, P.J. Withers, G.J. Baxter, Inertia Welding Nickel-Based Superalloy: Part II. Residual Stress Characterization, *Metall. Mater. Trans. A.* 33A (2002) 3227–3234.
22. K. Ma, R. Goetz, Modeling of Residual Stress and Machining Distortion in Aerospace components, AFRL-RX-WP-TP-2010-4152. (2010).
23. X. Nguyen-dinh, Phase Stable Single Crystal Materials, 177793, 1990.
24. K. An, H.D. Skorpenske, A.D. Stoica, D. Ma, X. Wang, E. Cakmak, First In Situ Lattice Strains Measurements Under Load at VULCAN, *Metall. Mater. Trans. A.* 42 (2011) 95–99. <https://doi.org/10.1007/s11661-010-0495-9>.
25. D. Sieborger, H. Knake, U. Glatzel, Temperature dependence of the elastic moduli of the nickel-base superalloy CMSX-4 and its isolated phases, *Mater. Sci. Eng. A.* 298 (2001) 26–33.
26. MATLAB and Imaging Processing Toolbox Release 2015a, (n.d.).
27. S.M. Adedayo, M.B. Adeyemi, Effect of Preheat on Residual Stress Distributions in Arc-Welded Mild Steel Plates, *J. Mater. Eng. Perform.* 9 (2000) 7–11.
28. S. Zaefferer, The electron backscatter diffraction technique – A powerful tool to study microstructures by SEM, *JEOL News.* 39 (2004) 10–15.
29. M. Soucail, M. Marty, H. Octor, The Effect of High Temperature Deformation on Grain Growth in a PM Nickel Base Superalloy, *Superalloys 1996 (Eighth Int. Symp. (1996) 663–666*.
30. L. Feng, Y. Gencang, Stress-induced recrystallization mechanism for grain refinement in highly undercooled superalloy, *J. Cryst. Growth.* 231 (2001) 295–305.
31. N. Iqbal, J. Rolph, R. Moat, D. Hughes, M. Hofmann, J. Kelleher, G. Baxter, P.J. Withers, M. Preuss, A Comparison of Residual Stress Development in Inertia Friction Welded Fine Grain and Coarse Grain Nickel-Base Superalloy, *Metall. Mater. Trans. A.* 42A (2011) 4056–4063. <https://doi.org/10.1007/s11661-011-0802-0>.
32. M.B. Prime, Cross-Sectional Mapping of Residual Stresses By Measuring the Surface Contour After a Cut, *J. Eng. Mater. Technol.* 836 (2001) 162–168.
33. M.B. Prime, R.J. Sebring, J.M. Edwards, D.J. Hughes, P.J. Webster, Laser surface contouring and spline data-smoothing for residual-stress measurement, *Exp. Mech.* 44 (2004) 176–184.

